ACS APPLIED MATERIALS & INTERFACES

Research Article

www.acsami.org

Polyethylenimine-Assisted Growth of High-Aspect-Ratio Nitrogen-Doped ZnO (NZO) Nanorod Arrays and Their Effect on Performance of Dye-Sensitized Solar Cells

Khalid Mahmood,* Bhabani Sankar Swain, Gill-Sang Han, Byeong-Jo Kim, and Hyun Suk Jung*

School of Advanced Materials Science & Engineering, Sungkyunkwan University, Suwon 440-746, Republic of Korea

ABSTRACT: The realization of arrays of high-aspect-ratio nitrogen-doped ZnO (NZO) nanorod is critical to the development of high-quality nanostructure-based optoelectronic and electronic devices. In this study, we used a solution-based method to grow arrays of vertically aligned high-aspect-ratio NZO nanorods on ZnO seed layer covered fluorine-doped tin oxide substrates. We investigated whether the diameters and aspect ratios of the nanorods were affected by the addition of polyethylenimine (PEI) to the precursor solution used as well as by variations in the growth temperature and the concentration of the precursor solution. The performances of dye-sensitized solar cells (DSSCs) in which the synthesized high-aspect-ratio NZO nanorods were used as the photoanode material were also studied. That the dopant, nitrogen, was introduced into the ZnO lattice was confirmed using X-ray photoelectron spectroscopy and energy-dispersive X-ray spectroscopy. It was seen that after the addition of PEI, the NZO and ZnO nanorod arrays increased in length and their diameters became smaller (i.e., their aspect ratios increased). This resulted in an increase in the amount of dye absorbed by them, leading to improvements in the DSSCs based on the nanorods. The structural, morphological, optical, and photovoltaic characteristics of ZnO and NZO nanorod arrays synthesized using different precursor concentrations and growth temperatures (160−190 °C) were also examined. We also investigated the effect of the use of PEI on these characteristics. The power conversion efficiency (PCE) of DSSCs fabricated using the NZO nanorod arrays was found to be significantly higher than that of DSSCs based on the pure ZnO nanorod arrays. This increase in efficiency could be attributed to the combined effects of the increase in the charge-carrier concentration, change in morphology, and increase in the Fermi energy levels of the nanorods, which resulted because of N doping. A PCE of 5.0% was obtained for a DSSC based on a film of arrays of NZO nanorods having an aspect ratio of ∼47 and synthesized using PEI.

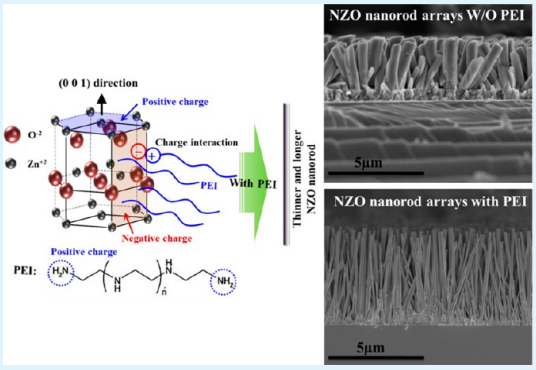

KEYWORDS: *zinc oxide, doping, aspect ratio, polyethylenimine, hydrothermal crystal growth, dye-sensitized solar cell*

1. INTRODUCTION

Vertically aligned ZnO nanorods have attracted a significant attention owing to their one-dimensional (1-D) structure and excellent properties.[1−4] In recent years, nanoscale 1D ZnO nanomaterials, i.e., nanowires and nanorods, have been investigated extensively because of their potential for use in light-emitting diodes, photodetectors, ultraviolet lasers, surface acoustic wave instruments, gas sensors, and solar cells.[5−11] The ability to synthesize functional ZnO nanomaterials having highly oriented and aligned structures will play a crucial role in the development of high-quality electronic devices. In particular, in the case of energy-conversion devices such as dye-sensitized solar cells (DSSCs), the fact that ZnO nanomaterials exhibit an electron-injection route and a bang-gap energy (3.37 eV at 298 K) similar to those of TiO_2 makes the nanomaterials even more interesting.[12] Moreover, because of the simplicity of their growth techniques and their high electronic mobilities, ZnO-based nanostructures have proven to be better suited as photoelectrode materials for DSSCs than those of TiO_2.[13]

The technological limits of the state-of-the-art DSSCs can be overcome by using vertically aligned ZnO or TiO_2 nanoarrays. These are synthesized directly on the surfaces of substrates coated with a transparent conductive oxide by replacing a disordered or particulate mesoporous thin film. Such arrays have been used as photoanode materials in DSSCs,[14,15] as they can improve the transport of electrons and promote the penetration of thick chemicals (such as ionic liquids, solid-type electrolytes, and quantum dots) and solid particles far more than can particulate or disordered thin films. A number of studies have been performed on DSSCs based on vertically aligned 1-D nanomaterials such as nanorods and nanowires, because of higher electron-transport rates, which result from the vertical alignment of the single-crystalline nanostructures.[16−21] However, the power conversion efficiency (PCE) of DSSCs based on 1D ZnO nanorods is relatively lower than

Received: January 6, 2014
Accepted: June 9, 2014
Published: June 18, 2014

that of their nanoparticle-based counterparts.[22−26] This is essentially because 1D ZnO nanorods have a lower surface area than nanoparticulate films, resulting in less dye adsorption and subsequently a poorer light-harvesting capability. These drawbacks can be overcome by enhancing the number density or the aspect ratio of the 1D nanostructures. However, this remains a challenging task.

Even though a large number of reports have been published on ZnO nanorod arrays in the last ten years, synthesizing ultralong and highly crystalline ZnO rods is still difficult. Arrays of ultralong ZnO nanowire arrays 85−180 μm in length have been synthesized by a vapor−liquid−solid method, physical vapor deposition, and chemical vapor deposition. However, these growth techniques are expensive, require the use of catalysts, involve high reaction temperatures, and can only be performed on a limited number of substrates.[27−29] To overcome these drawbacks, we can use the hydrothermal route, which is an aqueous solution-based bottom-up process, for growing well-aligned ZnO nanorod arrays, as the method involves lower temperatures and is inexpensive and simple. In addition, the morphology of the synthesized nanorods can be better controlled by varying the growth conditions, such as the growth temperature and time and the concentration of the precursor and other chemicals used.[30]

In earlier studies, the hydrothermal growth of ZnO arrays was generally performed using equimolar aqueous solutions of $Zn(NO)_3$ and hexamethylenetetramine (HMTA). However, the rapid decomposition of HMTA leads to supersaturation and bulk homogeneous nucleation. As a result, rods greater than 4 μm in length could not be obtained in a single growth cycle.[31−33] To synthesize arrays of nanorods of the desired length, we had to repeat the growth process by refreshing the growth solution. As a result, the synthesis of arrays of ultralong ZnO nanorods become a time-consuming process.[34,35] In order for the grown rods to be of the desired length and crystal quality, their growth should occur in the critical-supersaturation stage, during which homogeneous nucleation is suppressed and the growing units are supplied consistently.[36−38] It has been recently reported that polyethylenimine (PEI) aids the solution-based growth of ZnO nanowire arrays, with the thus-synthesized rods reaching 20−40 μm in length.[39,40] It was reported that the use of PEI increased the aspect ratio of the synthesized rods, resulting in a larger surface area and therefore greater dye loading.[32] Arrays of ultralong ZnO nanorods have used by a number of researchers as photoanode materials for DSSCs; however, the efficiencies of such photoanodes remain very low. Further, previous studies suggest that well-aligned ZnO nanorod arrays can only be grown through a complex mechanism. In addition, it is still not possible to control the aspect ratio of the synthesized ZnO nanorod arrays with precision. In particular, in the case of nanorods grown by aqueous solution-based processes, it is crucial that the diameter of the nanorods remains unchanged when their length is increasing.

In addition to increasing the aspect ratio of the ZnO nanorods, it is also essential to be able to fabricate ZnO nanorod arrays that can be used to increase the efficiency of DSSCs. Anionic dopants such as N, As, and P are generally used to enhance the visible-light characteristics of ZnO nanomaterials. The dopant not only hinders the recombination of holes and electrons but also enhances the visible-light absorption by reducing the band gap energy.[41] However, theoretical studies have shown that N is the most suitable dopant for producing shallow acceptor levels in ZnO.[42,43] Furthermore, N has a suitable ionic radius, low toxicity, and low ionization energy and is easy to handle. Although nanorods of N-doped ZnO (or NZO nanorods) exhibit high aspect ratios, the significant improvement noticed in the power conversion efficiency (PCE) of DSSCs based on such nanorods is due to the improved electrical and optical properties of the nanorods. After doping with N, the charge-carrier concentration increases, resulting in an improvement in the electron-transport characteristics of arrays of the nanorods. Therefore, if one could fabricate arrays of NZO nanorods with high aspect ratios, the efficiency of ZnO-based DSSCs could be increased significantly.

In this study, we synthesized arrays of NZO nanorods with high aspect ratios using a two-step aqueous solution-based method. PEI was added in order to increase the aspect ratio of the NZO nanorods. By controlling the process parameters such as the growth temperature and the concentration of the precursor solution and by using PEI, the morphological, structural, and photoluminescence (PL) characteristics of the NZO nanorod arrays could be varied. In addition, the photovoltaic properties of the NZO nanorod arrays were measured. Finally, their electronic structures as well as the changes in their morphology are discussed.

2. EXPERIMENTAL SECTION

2.1. Materials Used. Zinc acetate dihydrate $Zn(O_2CCH_3)_2(H_2O)_2$, zinc nitrate hexahydrate ($Zn(NO_3)_2{\cdot}6H_2O$), polyethylenimine [PEI; $(C_2H_5N)_n$], ammonium acetate (CH_3COONH_4), and hexamethylenetetramine ($C_6H_{12}N_4$) were used as-received.

2.2. Growth of ZnO and NZO Nanorod Arrays. The ZnO and NZO nanorod arrays were grown through a two-step process, which involved the synthesis of ZnO seed layers through electrospraying and the growth of the NZO nanorods on the layers using a hydrothermal method. The seed layers of pure ZnO were deposited on fluorine-doped tin oxide (FTO) substrates through electrospraying.[44] The precursor solution was prepared by dissolving 0.05 M zinc acetate dihydrate in a solution of ethanol and water (30:70 v/v). The flow rate, applied voltage, and nozzle-to-substrate distance were 0.002 mL min^{-1}, 5.6 kV, and 4 cm, respectively. The solution spraying time was 60 min, and the substrate was maintained at a temperature of 250 °C.

During the second step, an equimolar solution (10 mM) of hexamethylenetetramine (HMTA) and zinc nitrate hexahydrate was formed in 100 mL of water, and 5 mM PEI was added to the solution under continuous magnetic stirring. Ammonium acetate was also added to the solution as a source of the dopant, N, in a concentration of 5 at%. The ZnO-seeded substrates were placed at the bottom of an autoclave which contained the above-described solution for growing the nanorods. The autoclave was placed in a laboratory oven, which was maintained at 190 °C for 6 h. The substrates with the grown nanorod arrays were the removed from the growth solution, rinsed with water to remove any remaining salts, and dried in air. To control the aspect ratio of the NZO nanorods, the growth temperature was varied from 160 to 190 °C and the precursor concentration changed from 5 to 20 mM. The effects of the addition of PEI were also examined. Unless specified otherwise, the growth temperature and time were kept constant at 190 °C and 6 h, respectively.

2.3. Fabrication and Performance Measurement of DSSCs. The NZO and ZnO nanorod arrays synthesized on FTO substrates were immersed in a 0.5 mM solution of $(Bu_4N)_2[Ru(4,4\text{-}(COOH)\text{-}2,2,\text{-bipyridine})_2(NCS)_2]$ (N719 dye) in a 1:1 mixture of acetonitrile/*tert*-butyl alcohol mixture overnight. Pt-coated FTO substrates were used as counter electrodes. These were prepared by sputtering Pt onto FTO glass substrates for 10 s using a sputter current of 40 mA. An electrolyte solution composed of 0.4 M *tert*-butylpyridine, 0.1 M iodide (I_2), 0.1 M lithium iodide (LiI), and 0.5 M tetrabutylammo-

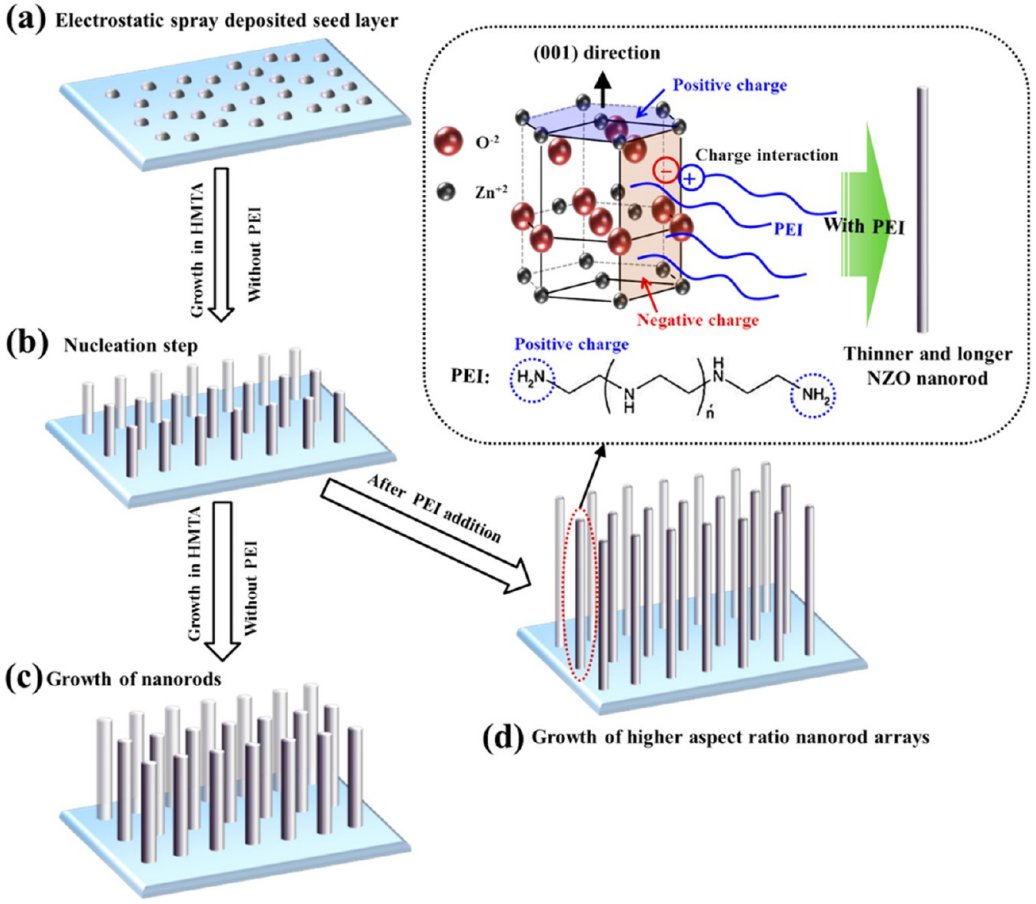

Figure 1. Various stages of growth of ZnO and NZO nanorod arrays with and without PEI: (a) seed layer deposited by electrospraying, (b) nucleation stage, (c) final growth of the nanorods, and (d) growth of high-aspect-ratio nanorods by using PEI (schematic representation of the effect of PEI on NZO nanorod growth).

nium iodide in acetonitrile was injected into the cells. To prevent the electrolyte from leaking, the hole was covered with a small glass square. The current density–voltage (J–V) data for the prepared cells were obtained under AM 1.5G simulated sunlight (model 67005, Oriel). The amounts of dye adsorbed were determined by measuring the ultraviolet–visible (UV–vis) spectra of the dye samples desorbed from the photoelectrodes. An M77250 monochromator (Oriel) was used to provide the monochromatic light. The incident photon-to-current efficiency (IPCE) values of the photoelectrodes were determined using the same potentiostat.

2.4. Characterization of ZnO and NZO Nanorod Arrays. Cross-sectional images of the nanorod arrays were obtained using field-emission scanning electron microscopy (FESEM) (model JSM-7100F, JEOL). The elemental compositions of the samples were determined using energy dispersive X-ray spectroscopy (EDS) (DX-4). The formation of the ZnO phase was confirmed through X-ray diffraction (XRD) analysis (Model M18XHF, Macscience Instruments). Transmission electron microscopy (TEM) (Tecnai G^2 F30 S-TWIN, FEI) was employed to characterize the microstructures of the nanorod arrays. The photoelectron spectra of the samples were obtained using X-ray photoelectron spectroscopy (XPS) (Sigma Probe, Thermo VG Scientific). The room-temperature photoluminescence characteristics of the samples were measured using a photoluminescence device (Horiba Jobin Yvon, France) that was excited using the 325 nm line from a He–Cd laser.

3. RESULTS AND DISCUSSION

The growth processes of the ZnO and NZO nanorod arrays with and without the addition of PEI are shown schematically in Figure 1. It can be seen that the presence of the ZnO seed layer is critical for the growth of high-density nanorod arrays because the seeds (Figure 1a) contained within the ZnO film provide the path for the growth of the nanorod arrays. It can be seen from the growth mechanism reactions that the growth of the $Zn(OH)_2$ units was followed by the production of hydroxyl ions by HMTA. Hence, the constant generation of OH^- and Zn^{2+} ions by the HMTA and zinc nitrate precursor solutions continuously produced $Zn(OH)_2$, which was eventually transformed into ZnO nanocrystallites. These grew into well-aligned ZnO nanorod arrays along the c-axis.[45] The effects of the addition of PEI, used to control the lengths and diameters of the ZnO nanorods as well as their lateral growth, were also examined. It was found that, in the absence of PEI, the NZO nanorod arrays exhibited shorter lengths (and wider diameters) along the c-axis direction (Figure 1c). However, after the addition of PEI, NZO nanorod arrays with high aspect ratios could be grown (Figure 1d). It was thus concluded that, during the growth of the nanorod arrays, the PEI molecules in the protonated form were efficiently adsorbed over the nonpolar sides of the nanorod arrays, thus preventing their sidewise growth (as illustrated in the inset of Figure 1d).[49] In addition, PEI helped reduce the diameter of the rods and increase their length, as it was selectively absorbed on the lateral facets of the rods and chelated the Zn^{2+} ions.[40,46,47] ZnO has a polar hexagonal crystal structure, which is composed of a positive top Zn^{2+} plane (0 0 1), a negative basal O^{2-} plane (0 0 1^-), and nonpolar (1 1 0), (0 1 0), and (1 0 0) surfaces.[46] The (0 0 1) positive plane (as shown in the inset of Figure 1d) possesses

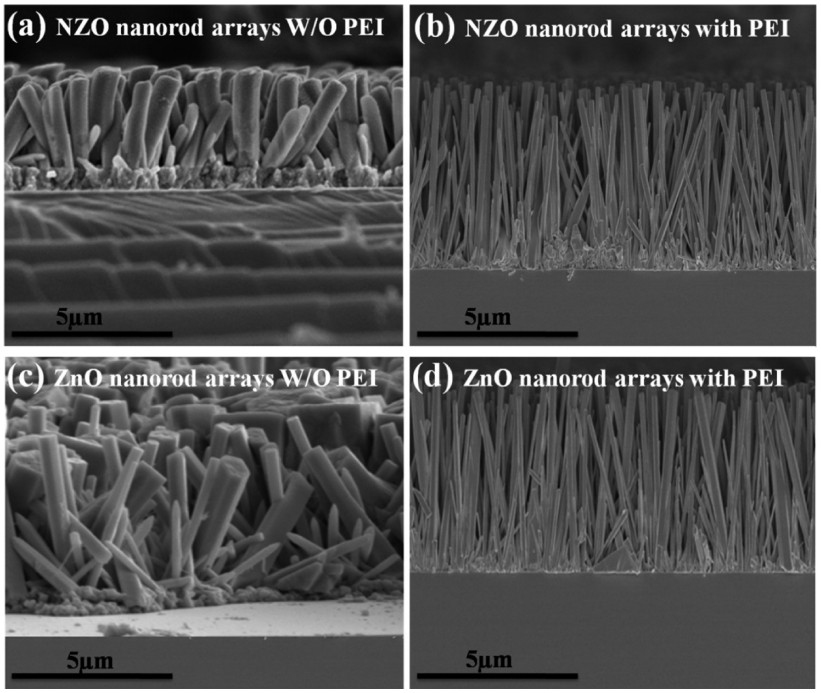

Figure 2. Cross-sectional FESEM images showing the effects of PEI addition on the growth of the NZO nanorod arrays: (a) nanorods grown without PEI and (b) with PEI. ZnO nanorod arrays (c) grown without PEI and (d) with PEI at 190 °C for 6 h.

Table 1. Effects of PEI Addition on the Aspect Ratios and Diameters of ZnO and NZO Nanorods Grown at 190 °C for 6 h; Photovoltaic Characteristics of Dye-Sensitized Solar Cells Based on the Synthesized ZnO and NZO Nanorod Arrays Are Also Shown[a]

	sample	aspect ratio	diameter (nm)	V_{OC} (mV)	J_{SC} (mA cm^{-2})	FF (%)	PCE (%)	adsorbed dye (× 10^{-7} mol cm^{-2})
NZO	with PEI	47 ± 2	150 ± 5	620 ± 2	15.0 ± 1	53.0 ± 2	5.0 ± 0.1	5.83 ± 0.2
	without PEI	9 ± 1	332 ± 15	550 ± 2	07.0 ± 1	52.0 ± 1	2.0 ± 0.1	2.14 ± 0.1
ZnO	with PEI	46.8 ± 1	151 ± 5	550 ± 1	08.0 ± 2	51.0 ± 2	2.2 ± 0.1	2.65 ± 0.1
	without PEI	8.7 ± 2	335 ± 15	350 ± 2	02.0 ± 1	52.0 ± 1	0.3 ± 0.1	0.5 ± 0.2

[a]Average performance (mean values) was calculated for 15 devices.

the highest surface energy. Therefore, faster crystal growth occurs in the *c*-axis direction. Moreover, PEI is a nonpolar polymer whose sides consist mainly of positively charged amino groups ($-NH_2$). It can therefore be readily protonated at pH values of 3−11. The positively charged PEI molecules were effectively adsorbed onto the lateral facets of the ZnO and NZO nanorod arrays because of electrostatic affinity.[46] Therefore, fewer rods grew in the lateral direction. Thus, PEI, which contained a large number of side amino groups, oriented toward the Zn ions, resulted in arrays of nanorods that exhibited smaller diameters and longer lengths and were better aligned that those obtained using other monomer capping agents.[46]

3.1. Effects of PEI Addition. Under controlled growth conditions (i.e., an equimolar precursor solution with a concentration of 10 mM, growth time of 6 h, and growth temperature of 190 °C), arrays of the NZO and ZnO nanorods were grown both with or without using PEI. Figure 2a shows cross-sectional FESEM images of NZO nanorod arrays grown without adding PEI. The rods have a typical length of ∼3.0 μm and diameters of 332 ± 15 nm (aspect ratio = ∼9.0). When PEI was used (Figure 2b), the aspect ratio increased significantly to ∼47 (i.e., the length increased to 7.0 μm while the diameters decreased to ∼150 ± 5 nm). Figure 2c shows a side view of the ZnO nanorod arrays grown without PEI; these nanorods have a length of ∼2.9 μm and diameters of 335 ± 15 nm (aspect ratio ≈ 8.9). However, after using PEI (Figure 2d, Table 1) the aspect ratio of the ZnO nanorods increased to ∼46.8 (i.e., the length increased to 6.9 μm and the diameters decreased to ∼151 ± 5 nm). As shown in Figure 2c, d, the addition of PEI also increased the aspect ratio of the pure ZnO nanorod arrays just as it did that of the NZO nanorods. The nanorods become thinner and taller after PEI was added.[32,50] The uniformity of both the ZnO and the NZO nanorod arrays increased significantly after the addition of PEI. Moreover, the verticality of the nanorods was also greater than that of the nanorods grown on a seed layer deposited using a sol solution heated to 60 °C.[49]

Figure 3 shows the XRD patterns of the NZO and ZnO nanorod arrays prepared with or without PEI. A high-intensity diffraction peak corresponding to the (0 0 2) plane of the hexagonal wurtzite structure of ZnO was noticed in all the patterns. This indicated that the nanorods grew along the *c*-axis direction and vertical to the substrate.[50] Moreover, the fact that the intensity of the (0 0 2) peak was higher when PEI was used proved that the aspect ratio of the NZO and ZnO nanorods as

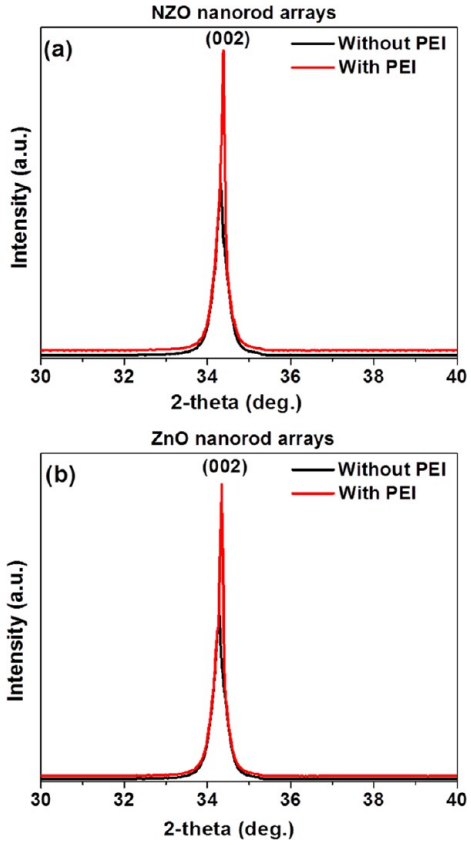

Figure 3. XRD patterns of (a) NZO and (b) ZnO nanorod arrays grown at 190 °C for 6 h with and without PEI.

well as their crystallinity improved with the use of PEI. The reason for the increase in the crystallinity after the addition of PEI was the growth of well-aligned, high-aspect-ratio ZnO and NZO nanorods along the *c*-axis direction. Similar effects of the addition of PEI on nanorod growth and orientation have been reported for ZnO nanorods grown by the hydrothermal route.[49] The fact that the XRD peaks corresponding to the nanorod arrays grown without PEI were less intense suggested that these rods had a lower crystallinity, which can be ascribed to the lower degree of vertical alignment of these nanorods along the *c*-axis. Furthermore, PEI also optimizes the seed layer present at the bottom of the nanorod arrays. It can be seen clearly in Figure 2b that the seed layer at the bottom of the nanorod arrays grown using PEI was thinner than the seed layer shown in Figure 2a, which corresponds to nanorods grown without PEI. When PEI is added to the growth solution, its degree of supersaturation is lowered. This hinders growth along the non-(0 0 2) directions.[47] In addition, the seed layer gets thinner because of the weak driving force, and the bottom ends of the nanorods are separated from each other, resulting in the growth of arrays of well-oriented, highly crystalline nanorods. In case when PEI is not used, the seed layer is thick, which causes the nanorods to fuse together at their bottom ends. This lowers the degree of vertical alignment of the nanorods and their crystallinity, which is reflected in the lower intensity of the (0 0 2) peaks. Because the atomic size of N is very similar to that of O, no peaks characteristic of N-doped ZnO were observed.

TEM analysis was performed to confirm the effect of PEI on the aspect ratio of the NZO nanorods. The resulting TEM images of the NZO nanorod arrays grown with and without PEI are shown in panels a and b in Figure 4, respectively. It can be seen that the differences in the aspect ratios are similar to those seen in the FESEM images (Figure 2a, b). The interplanar spacing of 0.52 nm is associated with the ZnO (002) plane. This confirmed that the nanorods grew preferentially along the [0001] direction.[48] The selected-area electron diffraction (SAED) patterns also confirmed that the NZO nanorods were single crystalline and had a wurtzite-like structure.

3.2. Effects of Precursor Concentration. Generally, an increase or decrease in the reactant concentrations will also affect the final products. Therefore, better control over the concentrations of the chemical reactants can help vary the dimensions of the final products. This was true in the case of the ZnO nanorods as well. With this fact in mind, the effects of the precursor solution concentration on the growth of the NZO and ZnO nanorod arrays was examined by varying the solution concentration from 5 to 20 mM in the presence of PEI and growing the nanorods at 180 °C for 3 h (Figure 5). The diameters of the NZO and the ZnO nanorods both decreased with the increase in the precursor concentration (Table 2). Compared with the other samples, the NZO and ZnO nanorod arrays grown using a concentration of 20 mM were more vertically oriented with respect to the substrate and exhibited higher aspect ratios. Moreover, the NZO nanorods exhibited a higher aspect ratio that did the ZnO nanorods. This indicates that N doping was effective in increasing the aspect ratio of the

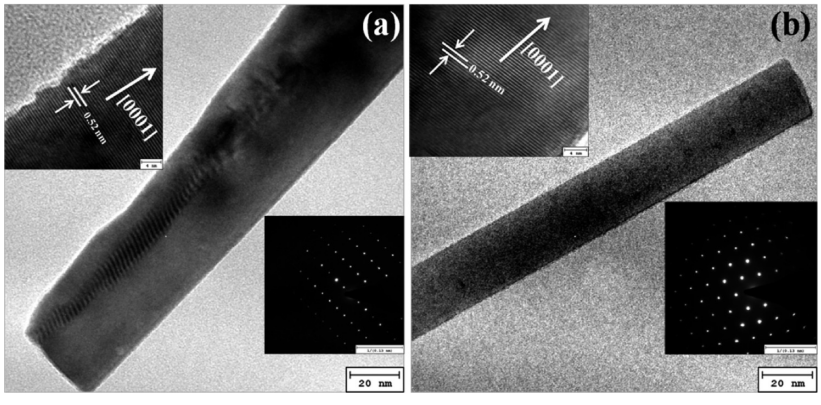

Figure 4. TEM images of a NZO nanorod grown (a) without PEI and (b) with PEI. The insets in the images are HRTEM images and SAED patterns of the NZO nanorods grown without and with PEI.

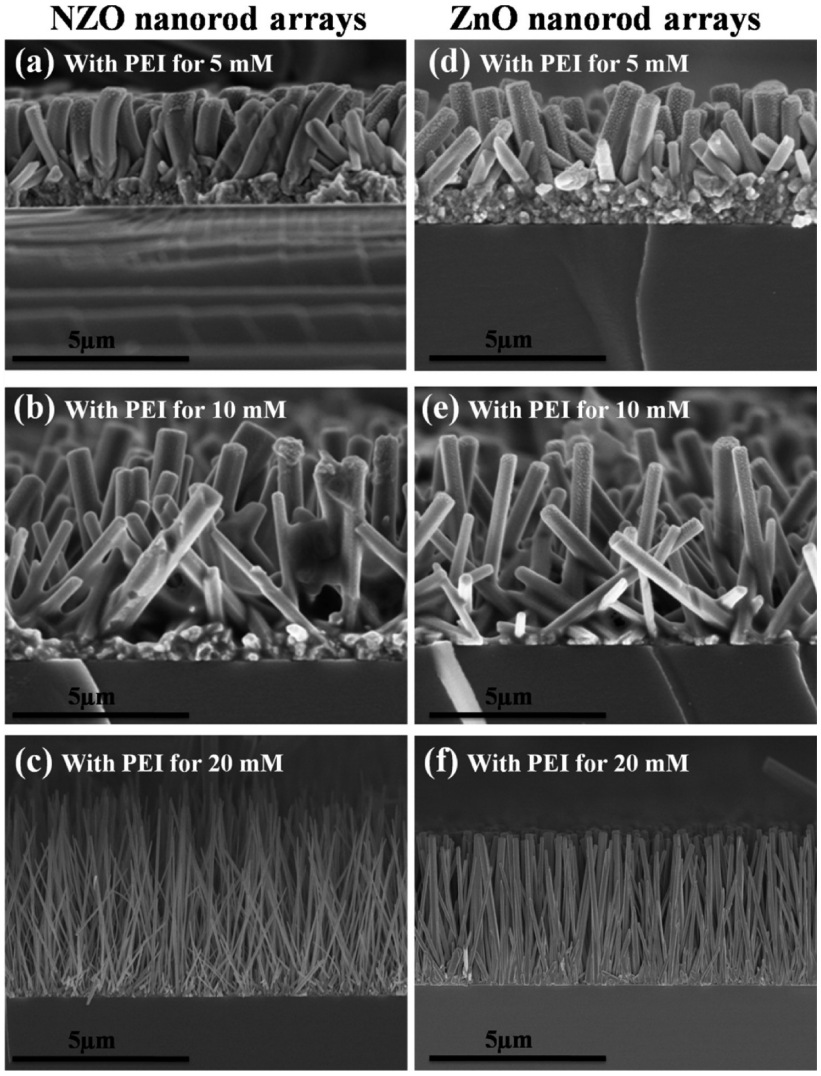

Figure 5. Typical FESEM images of NZO nanorod arrays fabricated using different precursor concentrations: (a) 5, (b) 10, and (c) 20 mM. ZnO nanorod arrays grown using precursor concentrations of (d) 5, (e) 10, and (f) 20 mM in the presence of PEI. The growth temperature was 180 °C and growth time was 3 h.

Table 2. Effects of Precursor Concentration on the Aspect Ratios and Diameters of the ZnO and NZO Nanorods Synthesized with and without PEI at 180 °C for 3 h; Photovoltaic Characteristics of Dye-Sensitized Solar Cells Based on the ZnO and NZO Nanorod Arrays Are Also Shown[a]

samples		concentration (mM)	aspect ratio	diameter (nm)	V_{OC} (mV)	J_{SC} (mA cm^{-2})	FF (%)	PCE (%)	adsorbed dye ($\times 10^{-7}$ mol cm^{-2})
	with PEI	5	4 ± 1	675 ± 10	600 ± 1	9.3 ± 1	50.5 ± 1	2.8 ± 0.1	2.93 ± 0.2
		10	15 ± 1	550 ± 10	600 ± 2	12.3 ± 1	51.0 ± 1	3.8 ± 0. 1	3.78 ± 0.2
		20	45 ± 1	155 ± 03	620 ± 1	13.7 ± 1	53.5 ± 1	4.5 ± 0.1	5.13 ± 0.2
NZO									
	without PEI	5	1.9 ± 2	850 ± 10	500 ± 1	4.5 ± 1	51.2 ± 1	1.2 ± 0.1	1.58 ± 0.2
		10	5.1 ± 1	830 ± 10	550 ± 1	5.5 ± 1	50.9 ± 1	1.5 ± 0.1	1.88 ± 0.2
		20	18.6 ± 1	350 ± 10	575 ± 1	7.0 ± 1	51.5 ± 1	2.0 ± 0.1	2.04 ± 0.2
	with PEI	5	3.9 ± 2	676 ± 10	475 ± 1	4.8 ± 1	50.0 ± 1	1.1 ± 0.1	1.43 ± 0.2
		10	10.1 ± 1	653 ± 10	550 ± 1	7.3 ± 1	51.5 ± 1	2.0 ± 0.1	2.71 ± 0.2
		20	43 ± 1	160 ± 10	550 ± 1	7.7 ± 1	51.5 ± 1	2.1 ± 0.1	2.95 ± 0.2
ZnO									
	without PEI	5	1.8 ± 1	852 ± 10	250 ± 1	1.5 ± 1	48.0 ± 1	0.18 ± 0.1	0.2 ± 0.2
		10	5.2 ± 2	829 ± 10	400 ± 1	2.5 ± 1	48.5 ± 1	0.49 ± 0.1	0.75 ± 0.2
		20	18.5 ± 1	353 ± 10	425 ± 1	4.0 ± 1	50.0 ± 1	0.85 ± 0.1	1.04 ± 0.2

[a]Average performance (mean values) was calculated for 15 devices.

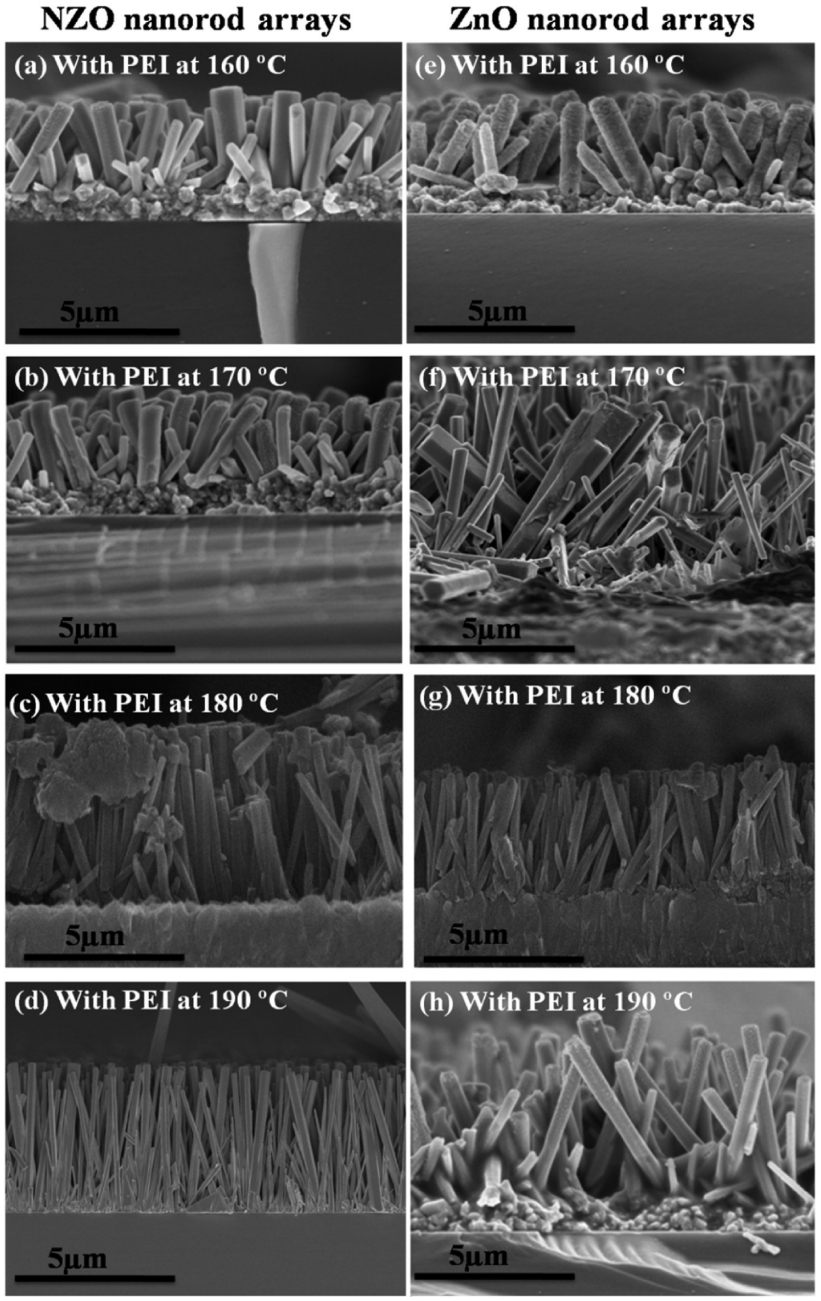

Figure 6. Typical FESEM images of NZO nanorod arrays grown at different temperatures: (a) 160, (b) 170, (c) 180, and (d) 190 °C. ZnO nanorod arrays grown at (e) 160, (f) 170, (g) 180, and (h) 190 °C in the presence of PEI using an equimolar precursor solution (10 mM) for 3 h.

nanorods in the presence of PEI. The reason for this is that doping with N also helps increase the length and decrease the diameter of ZnO nanorods.[45] Hence, the synergetic effects of the use of PEI and doping with N resulted in NZO nanorods exhibiting a higher aspect ratio than that of the pure ZnO nanorods. It is found that by optimizing the Zn^{2+}/OH^- concentrations, nanorods with a higher surface-to-volume ratio could be obtained. At low HMTA-to-$ZnNO_3$ ratios (i.e., at low precursor concentrations), nanostructures with larger diameter are grown; this can be ascribed to the generation of a greater number of NH_4^+ ions at the higher HMTA concentrations.[57] As a result of this, complexes such as $Zn(OH)_{4-x}(ONH_4)_2^{-x}$ are generated as the NH_4^+ ions stick to the $Zn(OH)_4^{2-}$ growth units of the nanorods, and $Zn(OH)_{4-x}(ONH_4)_2^{-x}$ is converted to $Zn(OH)_4^{2-}$, resulting in an increase in the growth rate.[57,58] This synthesis process is endothermic and restricts the growth of the nanorods in the <0 0 0 1> directions. Therefore, nanorods with larger diameters are grown at lower concentrations of the precursor.

3.3. Effects of Growth Temperature. Figure 6 shows cross-sectional FESEM images of the NZO and ZnO nanorod arrays grown at temperatures of 160−190 °C for 3 h; the precursor solution concentration was kept constant at 10 mM. The aspect ratios and diameters of the nanorod arrays are listed in Table 3. With an increase in the growth temperature from 160 to 190 °C, the NZO nanorods grown with and without PEI both exhibited an increase in their aspect ratio to 43.8 and 22.8, respectively. In the case of the ZnO nanorods grown with and without PEI, the increase in the growth temperature led to an increase in the aspect ratio to 43.2 and 22.6, respectively.

Table 3. Effects of the Growth Temperature on the Aspect Ratios and Diameters of ZnO and NZO Nanorod Arrays Grown with and without PEI Using a Precursor Solution with a Concentration of 10 mM for 3 h; Photovoltaic Characteristics of Dye-Sensitized Solar Cells Based on the ZnO and NZO Nanorod Arrays Are Also Shown[a]

samples		growth temperature (°C)	aspect ratio	diameter (nm)	V_{OC} (mV)	J_{SC} (mA cm^{-2})	FF (%)	PCE (%)	adsorbed dye (× 10^{-7} mol cm^{-2})
	with PEI	160	4.3 ± 1	700 ± 10	575 ± 1	8.0 ± 1	50.5 ± 1	2.3 ± 0.1	2.25 ± 0.2
		170	5.0 ± 1	690 ± 10	600 ± 1	10.5 ± 1	51.0 ± 1	3.2 ± 0.1	3.19 ± 0.2
		180	15 ± 1	550 ± 10	600 ± 2	12.3 ± 1	51.0 ± 1	3.8 ± 0.1	3.78 ± 0.2
		190	43.8 ± 1	160 ± 05	640 ± 1	13.3 ± 1	52.5 ± 1	4.5 ± 0.1	5.08 ± 0.2
NZO									
	without PEI	160	2.1 ± 1	855 ± 10	400 ± 1	2.5 ± 1	51.2 ± 1	0.5 ± 0.1	0.82 ± 0.2
		170	3.0 ± 1	840 ± 10	450 ± 1	4.0 ± 1	50.9 ± 1	0.9 ± 0.1	1.35 ± 0.2
		180	5.1 ± 1	830 ± 10	550 ± 1	5.5 ± 1	50.9 ± 1	1.5 ± 0.1	1.88 ± 0.2
		190	22.8 ± 1	300 ± 10	575 ± 1	6.0 ± 1	52.1 ± 1	1.8 ± 0.1	2.2 ± 0.2
	with PEI	160	4.2 ± 1	702 ± 10	450 ± 1	5.0 ± 1	51.0 ± 1	1.1 ± 0.1	1.44 ± 0.2
		170	4.9 ± 1	689 ± 10	500 ± 1	5.3 ± 1	49.5 ± 1	1.3 ± 0.1	1.74 ± 0.2
		180	10.1 ± 1	653 ± 10	550 ± 1	7.3 ± 1	51.5 ± 1	2.0 ± 0.1	2.71 ± 0.2
		190	43.2 ± 1	163 ± 5	575 ± 1	9.3 ± 1	52.0 ± 1	2.8 ± 0.1	2.95 ± 0.2
ZnO									
	without PEI	160	2.1 ± 1	854 ± 10	275 ± 1	1.2 ± 1	51.2 ± 1	0.17 ± 0.1	0.15 ± 0.2
		170	2.9 ± 1	843 ± 10	325 ± 1	1.5 ± 1	50.9 ± 1	0.25 ± 0.1	0.30 ± 0.2
		180	5.2 ± 2	829 ± 10	400 ± 1	2.5 ± 1	48.5 ± 1	0.49 ± 0.1	0.75 ± 0.2
		190	22.6 ± 1	302 ± 10	450 ± 1	5.0 ± 1	52.1 ± 1	1.13 ± 0.1	1.51 ± 0.2

[a]Average performance (mean values) was calculated for 15 devices.

However, with the increase in the growth temperature from 160 to 190 °C, the diameter of the nanorods decreased to 163 nm when PEI was used and to 302 nm when it was not. In addition, in the presence of PEI, the aspect ratio increased from 4.2 to 43.2, whereas in the absence of PEI, it increased from 2.1 to 22.6, on increasing the growth temperature, because PEI aids the deposition of ZnO, the decomposition of ammonium acetate in the solution, and the resulting chemical reaction. By increasing the growth temperature from 160 to 190 °C, the limits to mass transfer are overcome. This causes the diameter of the nanorods to decrease and their length to increase, because higher temperatures result in higher chemical reaction rates. To achieve efficient nitrogen doping, the self-compensating effect attributable to intrinsic defects, such as zinc interstitials and oxygen vacancies, should be prevented. During the growth of arrays of NZO nanorods at higher temperatures (160−190 °C), ammonium acetate, which is employed as the source of the dopant, N, undergoes sublimation and breaks down into N_2, NO, NO_2, and O_2. Thus, the properties of the obtained NZO nanorods depend mainly on the balance between the formation of donor defects by NO_2 molecules and the formation of acceptor defects by NO molecules. The higher N chemical potentials caused by molecular doping minimize the defect-formation energy. At low temperatures, ammonium acetate does not decompose into smaller constituents. As a result, it becomes harder to introduce the dopant, N, into the ZnO sites.

The XRD patterns for (a) NZO and (b) ZnO nanorod arrays grown using PEI are plotted as functions of the growth temperature in Figure 7. It can be seen that the intensity of the (0 0 2) peak increased with the growth temperature, because the length of the NZO nanorods increased linearly (i.e., the aspect ratio increased from ∼4.3 to 43.8) with the increase in the growth temperature (Table 3). Further, the same trend was observed in the case of the ZnO nanorods. In addition, the strong peak of the (0 0 2) plane corresponded to the hexagonal wurtzite phase. This proved that arrays of vertically aligned, high-aspect-ratio NZO nanorods were grown successfully.

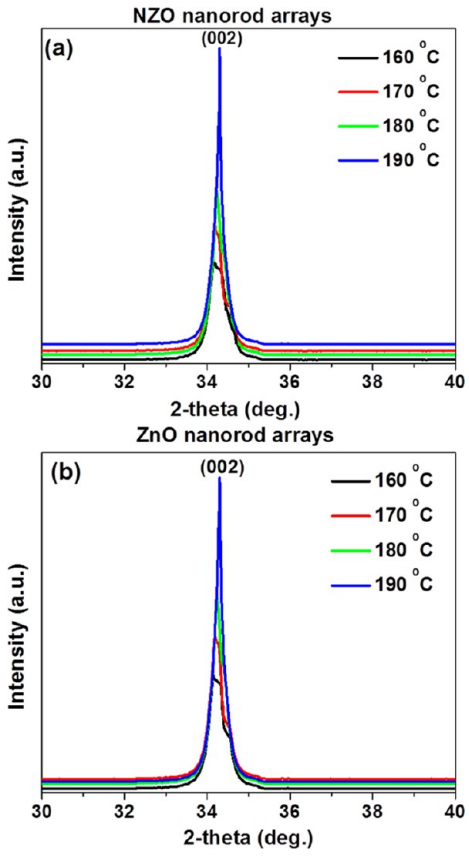

Figure 7. XRD patterns of (a) NZO and (b) ZnO nanorod arrays grown using an equimolar precursor solution (10 mM) containing PEI for 3 h at different growth temperatures.

3.4. Photoluminescence and Photovoltaic Characteristics of the Synthesized Nanorods. The room-temperature

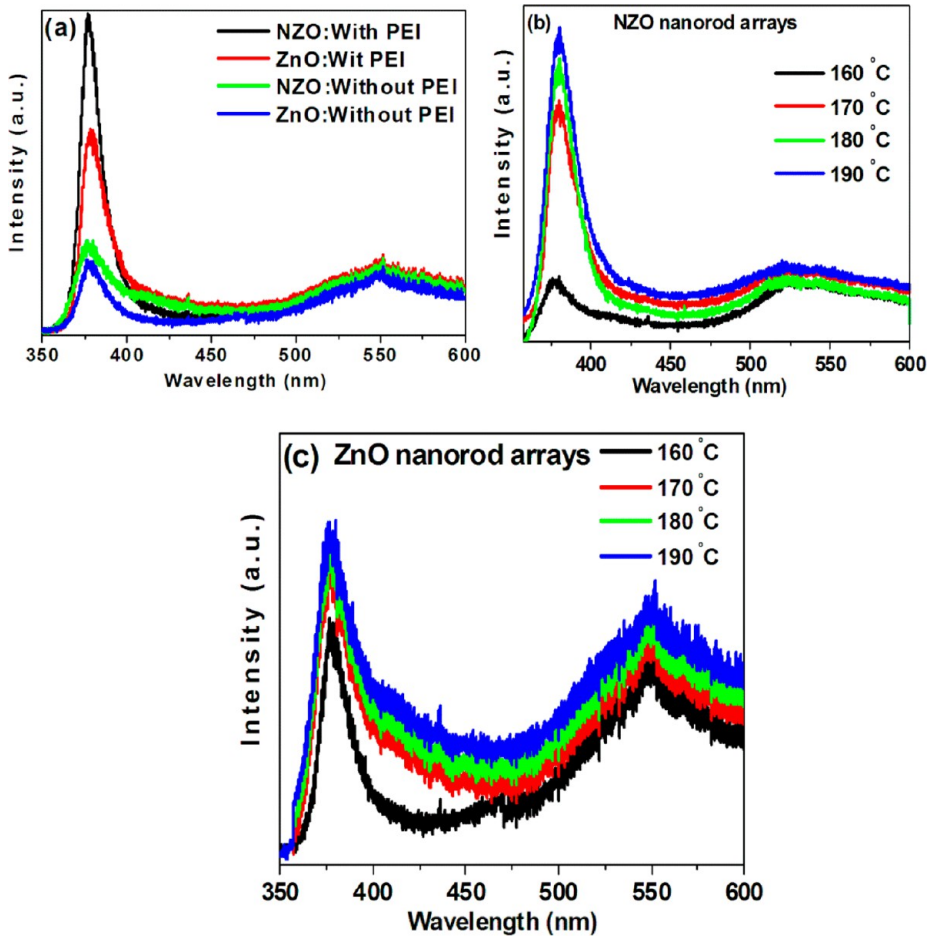

Figure 8. Room-temperature PL spectra of (a) NZO and ZnO nanorod arrays grown at 190 °C for 6 h with and without PEI. (b) NZO and (c) ZnO nanorod arrays grown using an equimolar precursor concentration (10 mM) for 3 h using PEI at different growth temperatures.

photoluminescence (PL) spectra of the synthesized ZnO nanorod arrays were measured to investigate the effects of N doping on the optical quality of the arrays. Generally, the PL spectrum of ZnO exhibits two emission bands. One of them exists in the UV range and is related to exciton emission, whereas the other is in the visible range and is caused by electron−hole recombination, which is attributable to the zinc interstitial defects and oxygen vacancies.[51] The effects of PEI on the PL spectra of NZO and ZnO can be seen in Figure 8a. When PEI was not used, both the PL spectra contained a low-intensity UV emission peak at ∼378 nm. However, when PEI was used, the intensity of this UV emission peak was higher. In addition, a broad low-intensity green emission peak, usually seen in the case of high-quality ZnO films, was also detected at approximately 500−550 nm. It could be concluded that the ZnO and NZO nanorod arrays grown using PEI exhibited higher-intensity UV emissions as well as weak emissions in the visible range. This was indicative of the high-quality growth of the ZnO phase. The NZO nanorods exhibited higher-intensity UV emissions that did the ZnO nanorods, demonstrating that doping with N resulted in significant improvements in the crystalline quality of the synthesized nanorods. That is to say, they exhibited fewer structural defects, zinc interstitials, and oxygen vacancies. This is attributable to the adsorption of PEI over the surfaces of the nanorods. It is likely that this results in the passivation of the nanorod surfaces, which, in turn, suppresses emissions in the visible range.[52,53]

The effects of the growth temperature on the room-temperature PL spectra of the NZO and ZnO nanorod arrays synthesized using PEI are exhibited in panels b and c in Figure 8, respectively. As the reaction temperature was increased from 160 to 190 °C, a higher-intensity UV emission peak was noticed, indicating that arrays of high-aspect-ratio nanorods with perfect crystal orientation were grown. This meant that increasing the growth temperature not only improved the crystalline nature of the nanorod arrays but also enhanced their optical characteristics. It could also be concluded that the higher-intensity UV emission peaks in the PL spectra corresponded to the high-intensity peaks in the XRD patterns (Figure 7), which were attributable to the greater crystallinity and high aspect ratios of the ZnO and NZO nanorods. The small defects in the nanorod arrays could be identified from the weak green emission peaks. The increase in the intensity of the UV emission peaks and decrease in the intensity of the visible-region emission peaks of the ZnO and NZO nanorod arrays on an increase in the temperature were caused by the preferential thermodynamic growth of highly crystalline ZnO nanorods.[49] In the present study, the OH^- ions to produce the $Zn(OH)_2$ phase were generated from HMTA. Therefore, the generation of $Zn(OH)_2$ nuclei and their conversion into the ZnO crystal phase could not occur at lower growth temperatures (i.e., at 160 and 170 °C). This resulted in the formation of arrays of ZnO nanorods of low crystallinity. On the other hand, when the growth temperature was increased (i.e., at 180 and 190 °C),

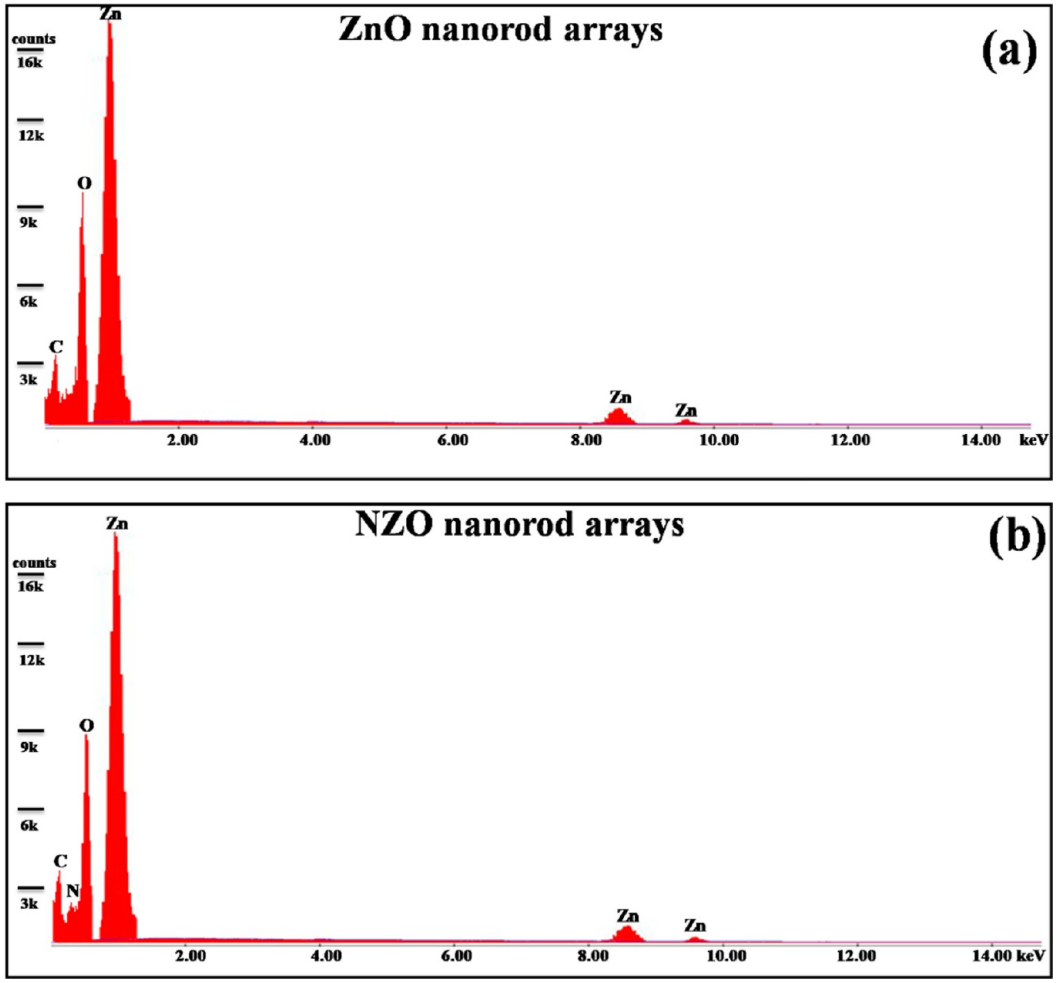

Figure 9. EDS spectra of (a) pure ZnO and (b) NZO nanorod arrays grown using an equimolar precursor solution (10 mM) for 6 h at 190 °C in the presence of PEI.

the growth of ZnO nanorod arrays was fast. Further, their structural defects were eliminated. That is to say, their crystalline quality was improved. These results are in good agreement with those of a previously reported study.[49] It can be therefore be concluded that increasing the growth temperature will significantly improve the optical properties of NZO and ZnO nanorods such that these properties can be tuned and the resulting nanorod arrays are suitable for use in field-emission and optoelectronic devices.

The typical EDS patterns for the ZnO and NZO (5 at%) nanorod arrays grown using a solution concentration of 10 mM, growth time of 6 h, and growth temperature of 190 °C in the presence of PEI are shown in panels a and b in Figure 9, respectively. The pattern in Figure 9a suggested the existence of Zn and O only in the ZnO nanorod arrays. The pattern also indicated that the ZnO nanorod arrays were phase pure. On the other hand, the pattern in Figure 9b suggested the coexistence of Zn, N, and O in the NZO nanorod arrays, demonstrating that N atoms have been substituted into the ZnO lattice.

The substitution of N into the ZnO lattice in the case of the NZO nanorod arrays was also confirmed using XPS analysis, as shown in Figure 10. That the N 1s peak appeared at 398.8 eV demonstrated the presence of N in the ZnO lattice, as shown in Figure 10a. In addition, two peaks at 1022.4 and 1045.5 eV, which corresponded to Zn $2p_{3/2}$ and Zn $2p_{1/2}$, respectively, were also noticed, as shown in Figure 9b. Furthermore, Figure 10c shows the O 1s spectrum, which exhibited a peak at 532.1 eV. This peak could be assigned to the oxidized metal ions, specifically the O−Zn and O−N ions, in the ZnO lattice, indicating that the structure of the valence band states was significantly affected by the N doping. Thus, the substitution of N into the lattice of the ZnO nanorods was also confirmed by the XPS data.

The current density−voltage (J−V) characteristics of DSSCs assembled using the synthesized high-aspect-ratio NZO and ZnO nanorod arrays grown with and without using PEI (Figure 2) are compared in Figure 11a. The photocurrent density (J_{sc}), fill factor (FF), open circuit voltage (V_{oc}), and power conversion efficiency (PCE) values of the cells are listed in Table 1. Increases in J_{sc} and PCE were noticed with an increase in the nanorod aspect ratio or length. When PEI was used, the longer nanorods resulted in greater dye loading and therefore, J_{sc} and PCE also increased. The DSSC based on NZO nanorods arrays fabricated using PEI exhibited the highest PCE of 5.0% (J_{sc} = 15 mA cm^{-2}); this was more than twice the PCE (2.10%) of a DSSC based on 33-μm-long ZnO nanowires grown using liquid-phase deposition.[39] Moreover, this PCE value of 5.0% was significantly higher than the PCE value of only 0.79% measured in the case of a DSSC based on long, vertically aligned ZnO nanowires grown through an ultrafast microwave-assisted hydrothermal method.[55] Furthermore, the highest PCE of 5.0% was also higher than the efficiency

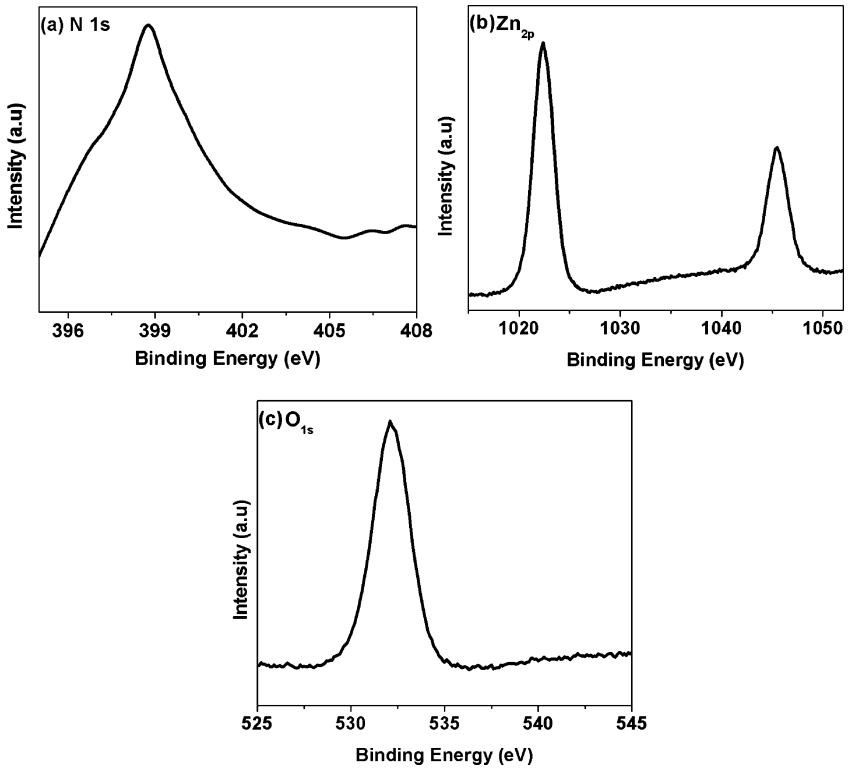

Figure 10. XPS spectra of the synthesized NZO nanorod arrays: (a) N 1s, (b) Zn 2p, and (c) O 1s.

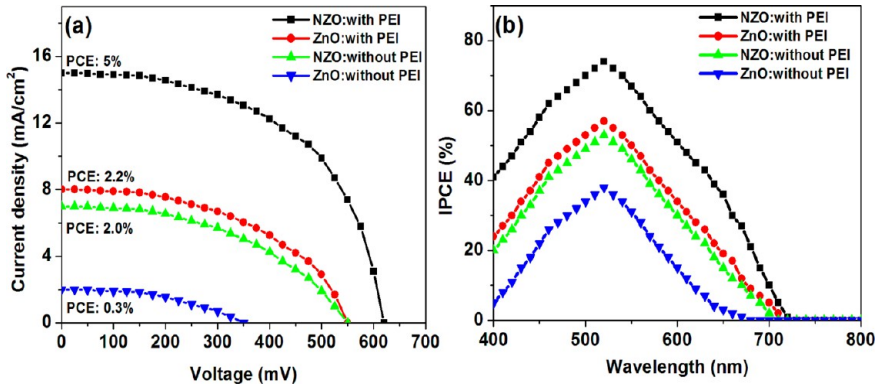

Figure 11. (a) Current−voltage curves and (b) IPCE spectra of the DSSCs based on the ZnO and NZO nanorod arrays synthesized with and without PEI at 190 °C for 6 h.

(2.30%) of a previously reported DSSC based on ZnO nanorods.[56] In addition, for the same aspect ratio and diameter, the cells based on the N-doped nanorod arrays exhibited better performance than that of the cells based on the undoped ZnO nanorod arrays. This was due to the combined action of the substitution of N atoms in the ZnO lattice and efficient photon-to-electron transfer in the cells. In addition to the increase in the dye-loading rate, the increases in Jsc and PCE after N doping were attributable to the increase in the charge-carrier density caused by the doping. An increase in the charge-carrier concentration in ZnO eventually facilitates electron transport, thereby increasing J_{sc}. The increase in Voc after doping could be attributed to improvements in the electron-transport property of the nanorods as well as to an increase in their Fermi energy levels, owing to the increase in the charge-carrier density.[54] Therefore, the N doping of the ZnO nanorods increased the PCE of DSSCs based on the nanorods. Generally, the amount of dye loaded in nanorods is determined by the surface area of the nanorods. The NZO nanorods had more uniform dimensions than did the ZnO nanorods. As a result, the NZO nanorods also exhibited a larger specific surface area and higher dye adsorption. The specific surface area of the synthesized ZnO nanorods was affected by the N doping of the nanorods. In the case of pure ZnO nanorods grown in the presence of PEI, the surface area was 49.0 $m^2\ g^{-1}$. However, the surface area of the N-doped nanorods was higher at 61.8 $m^2\ g^{-1}$. Upon the introduction of a small number of N atoms into the ZnO nanorods, their dye-loading rate increased significantly owing to the increase in their surface area. This means N doping played an important role in determining the dye-loading ability of ZnO nanorods. Further, along with the use of PEI, N doping also helped increase the aspect ratio of the ZnO nanorods, which further increased their surface area and hence their dye-loading rate. It has been reported that reducing the diameter of nanorods increases the surface area of photoelectrodes based on the nanorods, resulting in a greater degree

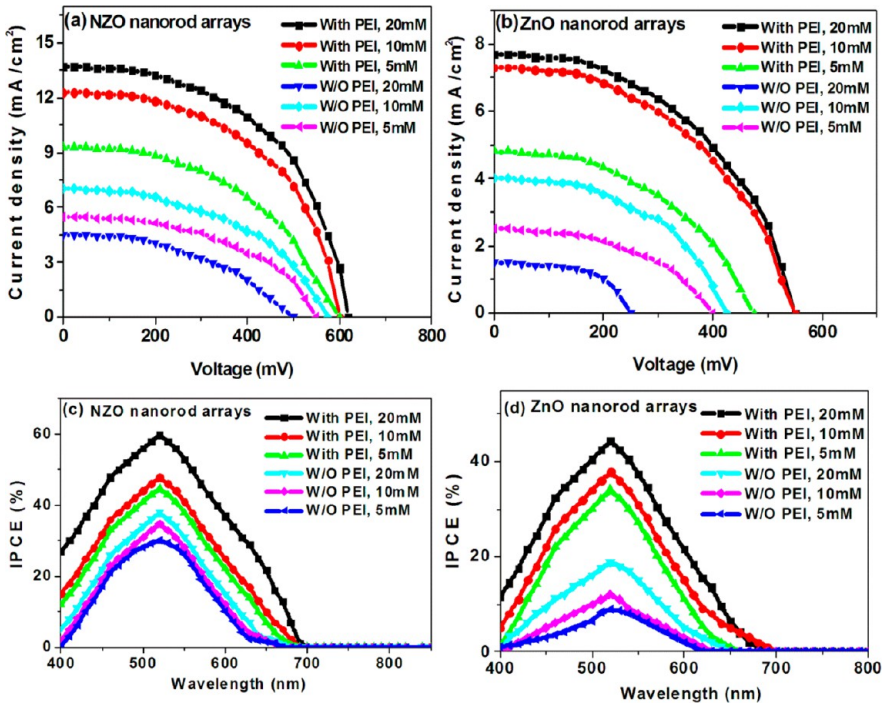

Figure 12. Current–voltage curves for DSSCS based on (a) NZO and (b) ZnO nanorod arrays and IPCE spectra of the DSSCS based on (c) NZO and (d) ZnO nanorod arrays grown with and without PEI at 190 °C for 3 h.

of dye loading.[59] Therefore, the NZO nanorod arrays exhibited greater dye loading than did the arrays of the pure ZnO nanorods. Moreover, the open spaces between adjacent nanorods aid electrolyte diffusion into the inner regions of the photoelectrodes, resulting in an increase in the redox-reaction rate of the electrolyte at the interface of the working electrode. Longer nanorods exhibit larger specific surface areas, resulting in an increase in the amount of dye adsorbed over the nanorod surfaces. This causes an increase in the PCE.

The V_{oc} of a DSSC is directly related to the electron concentration in the conduction band. The concentration is mainly determined by the rate of recombination of the conduction-band electrons with the I^{3-} ions in the electrolyte and with the oxidized dye molecules. The rate of recombination of the conduction-band electrons with the oxidized dye molecules is negligibly small and significantly slower than the rate of regeneration of the sensitizer by I^- ions,[44] Thus, in the case of the arrays of the NZO nanorods, which had a higher aspect ratio, the recombination rate of the conduction-band electrons was lower. Hence, the higher electron concentration in the conduction band and the reduction of the recombination rate resulted in an increase in Voc. In addition, Voc is also affected by the rate of recombination of separated charge carriers as well as by carrier accumulation at the interfaces. The higher V_{oc} observed in the case of the high-aspect-ratio ZnO nanorod arrays can also be accounted for by the increased charge collection at the ZnO/electrolyte interface both laterally (owing to the infiltration of a greater amount of the electrolyte) and vertically. In the case of the low-aspect-ratio ZnO nanorods, the amount of electrolyte that can infiltrate the spaces around adjacent ZnO nanorods is low. This limits the interfacial region and hence lateral charge collection. Further, the path length to be covered by charge carriers in the case of these nanorods before the carriers arrive at an interface is longer. This also accelerates carrier recombination, as the carriers encounter a greater number of defect centers. These two factors contributed to the low Voc noticed in the case of the low-aspect-ratio ZnO nanorod arrays. A few researchers have reported that V_{oc} can be increased by increasing the length of the nanorods or their aspect ratio.[55,56] Furthermore, the V_{oc} of a solar cell is a good indicator of whether the oxide semiconductor used in it is doped or not. The value of V_{OC} is determined by the difference between the Fermi level of the oxide semiconductor and the redox potential of the electrolyte. When the ZnO nanorods were doped with N, the V_{OC} of the cell based on them increased. The increase is attributable to the lower carrier recombination rate, higher amount of dye adsorbed on the surfaces of the nanorods, and faster transfer of electrons in the doped ZnO nanorods. In a previous study,[45] we had reported that the incorporation of N atoms into the ZnO lattice increases the Fermi level of the conduction band of ZnO, owing to an increase in the number of charge carriers, leading to a widening of the direct optical bandgap. We had also found that N doping raises the Fermi level of ZnO nanorods; this was in keeping with the results of another study.[60] The increase in the Fermi level of ZnO effectively enlarges the depletion region of the dye molecules, leading to improved charge extraction and higher device performance. The substitution of N at the oxide sites in the ZnO lattice increased the concentration of electrons. A few of these excess electrons fill the surface traps, causing an upward shift in the Fermi level. A higher Fermi level increases the V_{oc} value, as was noticed in the case of DSSCs based on the NZO nanorod arrays. Further, it also lowers the barrier for the efficient transfer of electrons.

To determine the cause for the higher photocurrent noticed in the case of the cells based on the high-aspect-ratio NZO nanorods, we determined the incident photon-to-current conversion efficiency (IPCE) spectra of the cells based on the NZO and ZnO nanorods (Figure 11b). It was found that

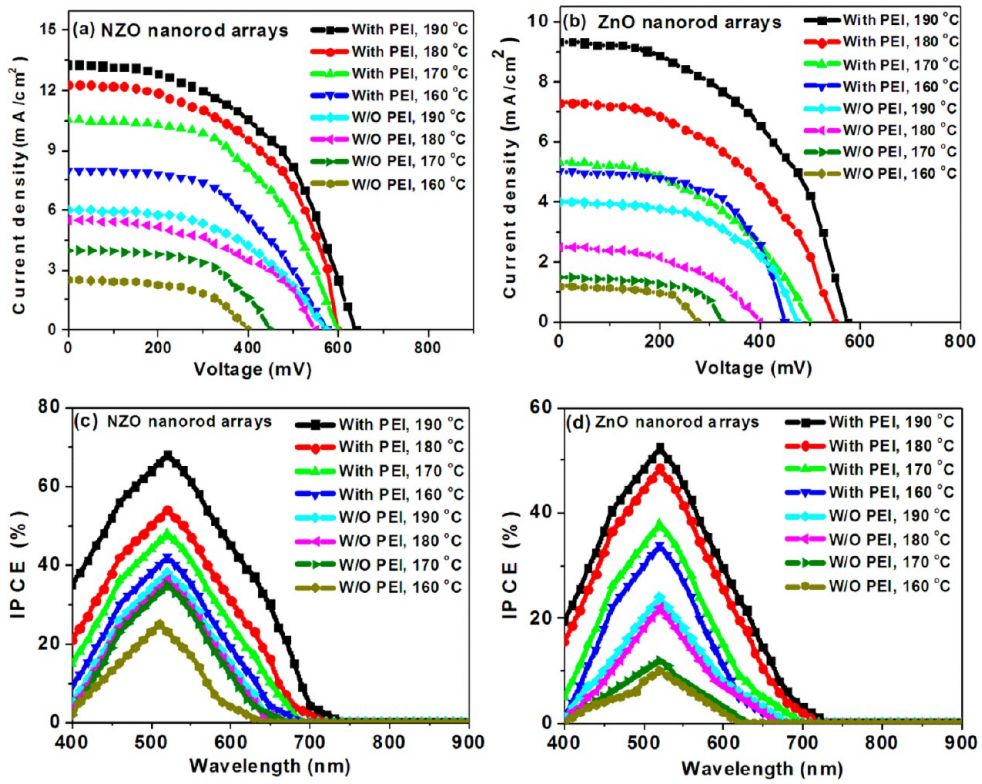

Figure 13. Current−voltage curves for DSSCs based on (a) NZO and (b) ZnO nanorod arrays and IPCE spectra of DSSCs based on (c) NZO and (d) ZnO nanorod arrays grown with and without PEI using an equimolar precursor solution (10 mM) for 3 h at different growth temperatures.

spectrum of the cell based on the NZO nanorods covered a wider range of wavelengths, indicating the incident light was utilized efficiently. The highest IPCE value at 520 nm was 74% for the DSSC based on the NZO nanorods synthesized using PEI, and it was 57% for the DSSC based on the ZnO nanorods fabricated using PEI. The higher IPCE for the NZO-based DSSC was due to the improved charge transport properties of the NZO nanorods as well as their better dye-loading properties, owing to their higher aspect ratio. For the DSSCs based on the NZO and ZnO nanorods synthesized without using PEI, the IPCE values at 520 nm were 53% and 38%, respectively. These are in accord with the J_{sc} values of the cells. The higher IPCE of the DSSC based on the high-aspect-ratio NZO nanorods proves that improvements in the PCE basically originate from efficient light scattering by the nanorod arrays because, in this case, the photons have a greater chance of being absorbed by the dye molecules.

Figure 12 shows the $J-V$ characteristics of the cells based on the high-aspect-ratio NZO and ZnO nanorod arrays as functions of the precursor concentration and whether PEI was used or not (shown above in Figure 5). The average photovoltaic characteristics of the cells are listed in Table 2. As the NZO nanorods grew longer and their aspect ratio increased after the addition of PEI, their dye-loading rate also increased. Therefore, the J_{sc} and PCE of the cells based on them also improved (Figure 12a). The value of J_{SC} increased owing to the increase in the aspect ratio of the nanorods. The increase in J_{SC} is related to the increase in the amount of dye adsorbed. The DSSC based on the NZO nanorods grown using a 20 mM precursor solution containing PEI and having an aspect ratio of ∼45.0 exhibited the highest PCE, which was 4.5%. With a decrease in the precursor concentration (10 to 5 mM), the PCE of the cell based on the NZO nanorods decreased from 3.8 to 2.8%, because the aspect ratio of the nanorods and hence the Jsc of the cell decreased. The cells based on the NZO nanorod arrays grown using PEI exhibited higher PCE values than did the cells based on the NZO nanorod arrays grown without using PEI, because PEI helped increase the aspect ratio of the nanorods, in turn, increased the Jsc and PCE of the corresponding cells. Moreover, as confirmed by the PL experiments, the passivation of the surfaces of the nanorods by the adsorption of PEI reduced the number of structural defects. This retarded charge recombination, resulting in increases in J_{sc} and V_{oc}. The same behavior was noticed in the case of the ZnO nanorod arrays (Figure 12b). A maximum PCE of 2.1% was obtained for the cell based on the ZnO nanorod arrays grown using a 20 mM precursor solution containing PEI and having an aspect ratio of ∼43.0. The cells based on the doped ZnO nanorod arrays exhibited higher PCE values than did the cells based on the undoped ZnO nanorod arrays, because the dopant, N, increased the photon-to-electron transfer rate in the cells. This increased the PCE. The IPCE spectra of the cells based on the NZO and ZnO nanorod arrays synthesized with and without PEI are shown as functions of the precursor concentration in panels c and d in Figure 12, respectively. The highest IPCE values at 520 nm were 60 and 44.5% for the DSSCs based on the NZO and ZnO nanorod arrays grown using a 20 mM precursor solution containing PEI. This was due to the high dye-loading rates of the nanorod arrays as well as to a decrease in the charge recombination rate in them. With a decrease in the precursor concentration (10 to 5 mM), the IPCE values also decreased, owing to the resultant decrease in the length and hence the aspect ratio of the nanorods. In addition, the cells based on the NZO nanorod arrays exhibited higher IPCE values compared to the cells based

on the undoped ZnO nanorod arrays, because the IPCE profile of the NZO cells was extended over a wider wavelength region.

Figure 13 shows the $J-V$ curves of the DSSCs based on the NZO and ZnO nanorods. The curves reflect the effects of the growth temperature on the photoelectrochemical performances of the cells. The Jsc, Voc, FF, and PCE values of the cells deduced from the $J-V$ curves (Figures 13a and 13b) are summarized in Table 3. For all the samples, the values of J_{sc} and the overall PCE increased drastically with an increase in the nanorod aspect ratio. Further, the results showed that reducing the diameter of the NZO and ZnO nanorods by increasing the synthesis temperature increased the surface areas of the nanorod-based photoelectrodes, resulting in a large dye-loading rate. Thus, the J_{sc} values of the DSSCs increased significantly. The significant increase in the PCE values of the cells was due to the larger internal surface area of the ZnO and NZO nanorods. This also resulted in greater diffusion of the electrolyte into the inner regions of the photoanode, owing to the presence of wide open spaces between adjacent nanorods. This caused the rate of the redox reaction at the interface of the working electrode to increase.[55] A significant increase in PCE of the DSSCs based on the NZO and ZnO nanorods because of the increase in their aspect ratios was noticed in the results. The DSSC based on the NZO nanorods grown at 190 °C using PEI and having an aspect ratio of ∼43.8 produced the highest PCE of 4.5%. With a decrease in the growth temperature (180 to 160 °C), the PCE of this DSSC decreased from 3.8 to 2.3%, because the aspect ratio of the NZO nanorods and hence the J_{sc} of the cell decreased. In addition, the low crystallinity of the nanorods grown at low temperatures may facilitate the charge-recombination process. This trend was noticed in the case of the ZnO nanorods (Figure 13b). The cells based on the NZO nanorod arrays showed higher PCE values than those of the cells based on the ZnO nanorod arrays, because after the N doping, the rate of recombination of the photoinjected electrons and the electrolyte redox species reduced. The IPCE spectra of the cells based on the NZO and ZnO nanorods synthesized with and without PEI are exhibited in Figure 13c, d, respectively, as functions of the growth temperature. The highest IPCE values at 520 nm were 68% and 38% for the DSSCs based on the NZO and ZnO nanorods grown using PEI at 190 °C; this was attributable to the larger surface areas of the nanorods, owing to their high aspect ratios. With a decrease in the growth temperature (180 to 160 °C), the IPCE values also decreased, because the lengths of the nanorods and hence their aspect ratios decreased. In addition, the cells based on the NZO nanorod arrays showed higher IPCE values than those of the cells based on the undoped ZnO nanorod arrays. This conclusion could be drawn because the IPCE profiles of the NZO nanorod-based cells were enhanced and extended over a wider wavelength region than were those of the cells based on the undoped ZnO nanorods. The improved electron collection in the NZO nanorod-based DSSCs resulted from the fact that the transport pathway for electrons in the well-aligned vertically arranged nanorods, which had a dense structure, was a straight one.

4. CONCLUSIONS

A simple solution-based process was devised for synthesizing high-aspect-ratio NZO nanorod arrays on FTO substrates using PEI such that that the nanorods grew preferentially along the *c*-axis direction and their lateral growth was inhibited. The addition of PEI had a positive effect in that the aspect ratio of the synthesized nanorods increased. It was also observed that, by varying the precursor concentration, the aspect ratio of the nanorods could be altered. The low density of defects in the NZO nanorods and their high crystallinity resulted in weak visible-range emissions and a strong UV emission peak. It was found that increasing the growth temperature and the precursor concentration helped enhance the structural, morphological, and PL properties of the nanorods, which, in turn, improved the performance of DSSCs based on the nanorods. Increasing the aspect ratio of the nanorods increased the intensity of their PL spectra. After the addition of PEI to the precursor solution, the aspect ratio of the nanorods increased, which resulted in greater dye adsorption and an improvement in the performance of the DSSCs based on them. A PCE of 5.0% was obtained for the DSSC based on the NZO nanorods with an aspect ratio of ∼47; these nanorods were synthesized using PEI. Finally, the IPCE spectra of the cells indicated that the electron-collection capability of the NZO nanorod-based anodes was higher. This is what resulted in improvements in the performance of the DSSCs based on the nanorods.

AUTHOR INFORMATION

Corresponding Authors

*E-mail: khalid@kaist.ac.kr.

*Tel: +82-31-290-7403. Fax: +82-31-290-7410. E-mail: hsjung1@skku.edu.

Notes

The authors declare no competing financial interest.

ACKNOWLEDGMENTS

This work was supported by grants from the National Research Foundation (NRF), which is funded by the Korean government (MEST) (2012M3A7B4049967, 2012M3A6A7054861 and 2014R1A4A1008474).

REFERENCES

(1) Nakahara, K.; Takasu, H.; Fons, P.; Yamada, A.; Iwata, K.; Matsubara, K.; Hunger, R.; Niki, S. Interactions Between Gallium and Nitrogen Dopants in ZnO Films Grown by Radical-source Molecular-beam Epitaxy. *Appl. Phys. Lett.* **2001**, *79*, 4139.

(2) Tang, Z. K.; Wong, G. K. L.; Yu, P.; Kawasaki, M.; Ohtomo, A.; Koinuma, H.; Segawa, Y. Room-temperature Ultraviolet Laser Emission from Self-assembled ZnO Microcrystallite Thin Films. *Appl. Phys. Lett.* **1998**, *72*, 3270.

(3) Ozgur, U.; Alivov, Y. I.; Liu, C.; Teke, A.; Reshchikov, M. A.; Dogan, S.; Avrutin, V.; Cho, S. J.; Morko, H. A Comprehensive Review of ZnO Materials and Devices. *J. Appl. Phys.* **2005**, *98*, 041301.

(4) Bagnall, D. M.; Chen, Y. F.; Zhu, Z.; Yao, T.; Koyama, S.; Shen, M. Y.; Goto, T. Optically Pumped Lasing of ZnO at Room Temperature. *Appl. Phys. Lett.* **1997**, *70*, 2230.

(5) Heo, Y. W.; Norton, D. P.; Tien, L. C.; Kwon, Y.; Kang, B. S.; Ren, F.; Pearton, S. J.; LaRoche, J. R. ZnO Nanowire Growth and Devices. *Mater. Sci. Eng. R* **2004**, *47*, 1.

(6) Huang, M. H.; Mao, S.; Feick, H. Q.; Yan, H. Q.; Wu, Y. Y.; Kind, H.; Weber, E.; Russo, R.; Yang, P. D. Room-temperature Ultraviolet Nanowire Nanolasers. *Science* **2001**, *292*, 1897.

(7) Rensmo, H.; Keis, K.; Lindstrolm, H.; Soldergren, S.; Solbrand, A.; Hagfeldt, A.; Lindquist, S. E.; Wang, L. N.; Muhammed, M. High Light-to-energy Conversion Efficiencies for Solar Cells Based on Nanostructured ZnO Electrodes. *J. Phys. Chem. B* **1997**, *101*, 2598.

(8) Liao, L.; Lu, H. B.; Li, J. C.; Liu, C.; Fu, D. J.; Liu, Y. L. The Sensitivity of Gas Sensor Based on Single ZnO Nanowire Modulated by Helium Ion Radiation. *Appl. Phys. Lett.* **2007**, *91*, 173110.

(9) Liang, S.; Sheng, H.; Liu, Y.; Hio, Z.; Lu, Y.; Shen, H. ZnO Schottky Ultraviolet Photodetectors. *J. Cryst. Growth* **2001**, *225*, 110.

(10) Hwang, D. K.; Kang, S. H.; Lim, J. H.; Yang, E. G.; Oh, J. Y.; Yang, J. H.; Park, S. J. p-ZnO/n-GaN Heterostructure ZnO Light-emitting Diodes. *Appl. Phys. Lett.* **2005**, *86*, 222101.
(11) Emanetoglu, N. W.; Zhu, J.; Chen, Y.; Zhong, J.; Chen, Y. M.; Lu, Y. C. Surface Acoustic Wave Ultraviolet Photodetectors using Epitaxial ZnO Multilayers Grown on r-plane Sapphire. *Appl. Phys. Lett.* **2004**, *85*, 3702.
(12) Furube, A.; Katoh, R.; Yoshihara, T.; Hara, K.; Murata, S.; Arakawa, H.; Tachiya, M. Ultrafast Plasmon-induced Electron Transfer from Gold Nanodots into TiO_2 Nanoparticles. *J. Phys. Chem. B* **2004**, *108*, 12583−12592.
(13) Ku, C. H.; Wu, J. J. Electron Transport Properties in ZnO Nanowire Array/nanoparticle Composite Dye-sensitized Solar Cells. *Appl. Phys. Lett.* **2007**, *91*, 93117.
(14) Michael, G. Dye-sensitized Solar Cells. *J. Photochem. Photobiol. C* **2003**, *4*, 145.
(15) Martinson, A. B. F.; Hamann, T. W.; Pellin, M. J.; Hupp, J. T. New Architectures for Dye-sensitized Solar Cells. *Chem.—Eur. J.* **2008**, *14*, 4458.
(16) Galoppini, E.; Rochford, J.; Chen, H. H.; Saraf, G.; Lu, Y. C.; Hagfeldt, A.; Boschloo, G. Fast Electron Transport in Metal Organic Vapor Deposition Grown Dye-sensitized ZnO Nanorod Solar Cells. *J. Phys. Chem. B* **2006**, *110*, 16159−16161.
(17) Gao, H. M.; Fang, G. J.; Wang, M. J.; Liu, N. S.; Yuan, L. Y.; Li, C.; Ai, L.; Zhang, J.; Zhou, C. H.; Wu, S. J.; Zhao, X. Z. The Effect of Growth Conditions on the Properties of ZnO Nanorod Dye-sensitized Solar Cells. *Mater. Res. Bull.* **2008**, *43*, 3345−3351.
(18) Lee, Y. M.; Yang, H. W. Optimization of Processing Parameters on the Controlled Growth of ZnO Nanorod Arrays for the Performance Improvement of Solid-state Dye-Sensitized Solar Cells. *J. Solid State Chem.* **2011**, *184*, 615−623.
(19) Wu, J. J.; Chen, G. R.; Yang, H. H.; Ku, C. H.; Lai, J. Y. Effects of Dye Adsorption on the Electron Transport Properties in ZnO-nanowire Dye-sensitized Solar Cells. *Appl. Phys. Lett.* **2007**, *90*, 213109.
(20) Pradhan, B.; Batabyal, S. K.; Pal, A. J. Vertically Aligned ZnO Nanowire Arrays in Rose Bengal-based Dye-sensitized Solar Cells. *Sol. Energy Mater. Sol. C* **2007**, *91*, 769−773.
(21) Gao, Y. F.; Nagai, M.; Chang, T. C.; Shyue, J. J. Solution-Derived ZnO Nanowire Array Film as Photoelectrode in Dye-sensitized Solar Cells. *Cryst. Growth Des.* **2007**, *7*, 2467−2471.
(22) Baxter, J. B.; Aydil, E. S. Nanowire-based Dye-sensitized Solar Cells. *Appl. Phys. Lett.* **2005**, *86*, 053114.
(23) Law, M.; Greene, L. E.; Johnson, J. C.; Saykally, R.; Yang, P. Nanowire Dye-sensitized Solar Cells. *Nat. Mater.* **2005**, *4*, 455.
(24) Mor, G. K.; Shankar, K.; Paulose, M.; Varghese, O. K.; Grimes, C. A. Use of Highly-ordered TiO_2 Nanotube Arrays in Dye-sensitized Solar Cells. *Nano Lett.* **2006**, *6*, 215.
(25) Liu, B.; Aydil, E. S. Growth of Oriented Single-crystalline Rutile TiO_2 Nanorods on Transparent Conducting Substrates for Dye-sensitized Solar Cells. *J. Am. Chem. Soc.* **2009**, *131*, 3985.
(26) Xu, C.; Shin, P. H.; Cao, L.; Wu, J.; Gao, D. Ordered TiO_2 Nanotube Arrays on Transparent Conductive Oxide for Dye-sensitized Solar Cells. *Chem. Mater.* **2010**, *22*, 143.
(27) Kuo, T. J.; Lin, C. N.; Kuo, C. L.; Huang, M. H. Growth of Ultralong ZnO Nanowires on Silicon Substrates by Vapor Transport and Their Use as Recyclable Photocatalysts. *Chem. Mater.* **2007**, *19*, 5143.
(28) Zhu, G.; Zhou, Y.; Wang, S.; Yang, R.; Ding, Y.; Wang, X.; Bando, Y.; Wang, Z. L. Synthesis of Vertically Aligned Ultra-long ZnO Nanowires on Heterogeneous Substrates with Catalyst at the Root. *Nanotechnology* **2012**, *23*, 055604.
(29) Wen, L.; Wong, K. M.; Fang, Y.; Wu, M.; Lei, Y. Fabrication and Characterization of Well-aligned High Density ZnO Nanowire Arrays and Their Realizations in Schottky Device Applications Using a Two-step Approach. *J. Mater. Chem.* **2011**, *21*, 7090.
(30) Yi, S. H.; Choi, S. K.; Jang, J. M.; Kim, J. A.; Jung, W. G. Low-temperature Growth of ZnO Nanorods by Chemical Bath Deposition. *J. Colloid Interface Sci.* **2007**, *313*, 705−710.
(31) Vayssieres, L. Growth of Arrayed Nanorods and Nanowires of ZnO from Aqueous Solutions. *Adv. Mater.* **2003**, *15*, 464.
(32) Greene, L. E.; Yuhas, B. D.; Law, M.; Zitoun, D.; Yang, P. Solution-grown Zinc Oxide Nanowires. *Inorg. Chem.* **2006**, *45*, 7535.
(33) Lee, Y. M.; Yang, H. W. Optimization of Processing Parameters on the Controlled Growth of ZnO Nanorods Arrays for the Performance Improvement of Solid-state Dye-sensitized Solar Cells. *J. Solid State Chem.* **2011**, *184*, 615−623.
(34) Hua, G.; Tian, Y.; Yin, L.; Zhang, L. Reproducible Growth of Ultralong ZnO Nanowire Arrays in the Metastable Supersaturated Solution. *Cryst. Growth Des.* **2009**, *9*, 4653.
(35) Qiu, J.; Zhuge, F.; Gao, X.; Gan, X.; Yu, W.; Li, X.; He, W.; Park, S.; Kim, H.; Hwang, Y. Solution-derived 40 μm Vertically Aligned ZnO Nanowire Arrays as Photoelectrodes in Dye-sensitized Solar Cells. *Nanotechnology* **2010**, *21*, 159602.
(36) Chen, L. Y.; Yin, Y. T. Facile Continuous Flow Injection Process for High Quality Long ZnO Nanowire Arrays Synthesis. *Cryst. Growth Des.* **2012**, *12*, 1055.
(37) Tian, J. H.; Hu, J.; Li, S. S.; Zhang, F.; Liu, J.; Shi, J.; Li, X.; Tian, Z. Q.; Chen, Y. Improved Seedless Hydrothermal Synthesis of Dense and Ultralong ZnO Nanowires. *Nanotechnology* **2011**, *22*, 245601.
(38) Richardson, J. J.; Lange, F. F. Controlling Low Temperature Aqueous Synthesis of ZnO. 2. A Novel Continuous Circulation Reactor. *Cryst. Growth Des.* **2009**, *9*, 2576.
(39) Xu, C.; Shin, P.; Cao, L.; Gao, D. Preferential Growth of Long ZnO Nanowire Array and Its Application in Dye-sensitized Solar Cells. *J. Phys. Chem. C* **2010**, *114*, 125.
(40) Qiu, J.; Li, X.; He, W.; Park, S. J.; Kim, H. K.; Hwang, Y. H.; Lee, J. H.; Kim, Y. D. The Growth Mechanism and Optical Properties of Ultralong ZnO Nanorod Arrays with a High Aspect Ratio by a Preheating Hydrothermal Method. *Nanotechnology* **2009**, *20*, 155603.
(41) Chen, L.-C.; Tu, Y.-J.; Wang, Y.-S.; Kan, R.-S.; Huang, C.-M. Characterization and Photoreactivity of N-, S-, and C-doped ZnO Under UV and Visible Light Illumination. *J. Phptochem. Photobiol. A: Chem.* **2008**, *199*, 170.
(42) Wang, L. G.; Zunger, A. Cluster-Doping Approach for Wide-gap Semiconductors: The Case of *p*-type ZnO. *Phys. Rev. Lett.* **2003**, *90*, 256401.
(43) Park, C. H.; Zhang, S. B.; Wei, S. H. Origin of *p*-type Doping Difficulty in ZnO: The Impurity Perspective. *Phys. Rev. B* **2002**, *66*, 073202.
(44) Mahmood, K.; Park, S. B. Highly Efficient Dye-sensitized Solar Cell With an Electrostatic Spray Deposited Upright-standing Boron-doped ZnO (BZO) Nanoporous Nanosheet-based Photoanode. *J. Mater. Chem. A* **2013**, *1*, 4826−4835.
(45) Mahmood, K.; Park, S. B. Growth and Conductivity Enhancement of N-doped ZnO Nanorod Arrays. *J. Cryst. Growth* **2012**, *347*, 104−112.
(46) Xu, C.; Gao, D. Two-Stage Hydrothermal Growth of Long ZnO Nanowires for Efficient TiO_2 Nanotube-based Dye-sensitized Solar Cells. *J. Phys. Chem. C* **2012**, *116*, 7236.
(47) Zhou, Y.; Wu, W.; Hu, G.; Wu, H.; Cui, S. Hydrothermal Synthesis of ZnO Nanorod Arrays with the Addition of Polyethyleneimine. *Mater. Res. Bull.* **2008**, *43*, 2113.
(48) Greene, L.; Law, M.; Goldberger, J.; Kim, F.; Johnson, J.; Zhang, Y.; Saykally, R.; Yang, P. Low Temperature Wafer-scale Production of ZnO Nanowires Arrays. *Angew. Chem., Int. Ed.* **2003**, *42*, 3031.
(49) Choi, H. S.; Vaseem, M.; Kim, G.; Im, Y. H.; Hahn, Y. B. Growth of High Aspect Ratio ZnO Nanorods by Solution Process: Effect of Polyethyleneimine. *J. Solid State Chem.* **2012**, *189*, 25.
(50) Qurashi, A.; Kim, J. H.; Hahn, Y. B. Density-Controlled Selective Growth of Well aligned ZnO Nanorod Arrays by a Hybrid Approach. *Superlattices Microstruct.* **2010**, *48*, 162−169.
(51) Zeng, H. B.; Cai, W. P.; Hu, J. L.; Duan, G. T.; Liu, P. S.; Li, Y. Violet Photoluminescence from Shell Layer of Zn/ZnO Core-shell Nanoparticles Induced by Laser Ablation. *Appl. Phys. Lett.* **2006**, *88*, 171910.
(52) Cheng, C. W.; Sie, E. J.; Liu, B.; Huan, C. H. A.; Sum, T. C.; Sun, H. D.; Fan, H. J. Surface Plasmon Enhanced Band Edge

Luminescence of ZnO Nanorods by Capping Au Nanoparticles. *Appl. Phys. Lett.* **2010**, *96*, 071107.
(53) Lide, D. R., Ed. *Chemical Rubber Company Handbook of Chemistry and Physics*, 81st ed.; CRC Press: Boca Raton, FL, 2000.
(54) Diamant, Y.; Chen, S. G.; Melamed, O.; Zaban, A. Core−Shell Nanoporous Electrode for Dye Sensitized Solar Cells: the Effect of the $SrTiO_3$ Shell on the Electronic Properties of the TiO_2 Core. *J. Phys. Chem. B* **2003**, *107*, 1977.
(55) Mahpeykar, S. M.; Koohsorkhi, J.; Ghafoori-fard, H. Ultra-Fast Microwave-assisted Hydrothermal Synthesis of Long Vertically Aligned ZnO Nanowires for Dye-sensitized Solar Cell Application. *Nanotechnology* **2012**, *23*, 165602.
(56) Huang, Q.; Fang, L.; Chen, X.; Saleem, M. Effect of Polyethyleneimine on the Growth of ZnO Nanorod Arrays and Their Application in Dye-sensitized Solar Cells. *J. Alloys Compd.* **2011**, *509*, 9456−9459.
(57) Polsongkrama, D.; Chamninok, P.; Pukird, S.; Chowb, L.; Lupan, O.; Chai, G.; Khallaf, H.; Park, S.; Schulte, A. Effect of Synthesis Conditions on the Growth of ZnO Nanorods Via Hydrothermal Method. *Physica B* **2008**, *403*, 3713−3717.
(58) Zhang, H.; Yang, D.; Yi, Y. J.; Ma, X. Y.; Xu, J.; Que, D. L. Low Temperature Synthesis of Flowerlike ZnO Nanostructures by Cetyltrimethylammonium Bromide-assisted Hydrothermal Process. *J. Phys. Chem. B* **2004**, *108*, 3955.
(59) Zhua, S.; Chena, X.; Zuoa, F.; Jianga, M.; Zhoua, Z.; Huib, D. Controllable Synthesis of ZnO Nanograss with Different Morphologies and Enhanced Performance in Dye-sensitized Solar Cells. *J. Solid State Chem.* **2013**, *197*, 69−74.
(60) Zheng, Y.-Z.; Ding, H.; Tao, X.; Chen, J.-F. Investigation of Iodine Dopant Amount Effects on Dye-sensitized Hierarchically Structured ZnO Solar Cells *Mater. Res. Bull.* DOI: http://dx.doi.org/10.1016/j.materresbull.2014.04.027.